Theor. Appl. Climatol. (2006)
DOI 10.1007/s00704-005-0201-9

Theoretical and Applied Climatology
Printed in Austria

[1] Instituto de Meteorología, La Habana, Cuba
[2] Universidade de São Paulo, São Paulo, Brasil
[3] Centro de Previsão do Tempo e Estudos Climaticos (CPTEC)/Instituto Nacional de Pesquisas Espaciais (INPE), São Paulo, Brasil
[4] Instituto Geofísico del Perú, Lima, Perú
[5] Iowa State University, Ames, Iowa, USA

Sensitivity studies of the RegCM3 simulation of summer precipitation, temperature and local wind field in the Caribbean Region

D. Martínez-Castro[1], R. Porfirio da Rocha[2], A. Bezanilla-Morlot[1], L. Alvarez-Escudero[1], J. P. Reyes-Fernández[3], Y. Silva-Vidal[4], and **R. W. Arritt[5]**

With 13 Figures

Received December 6, 2004; revised May 4, 2005; accepted August 10, 2005
Published online May 26, 2006

Summary

We present a preliminary evaluation of the performance of three different cumulus parameterization schemes in the ICTP Regional Climate Model RegCM3 for two overlapping domains (termed "big" and "small") and horizontal resolutions (50 and 25 km) in the Caribbean area during the summer (July–August–September). The cumulus parameterizations were the Grell scheme with two closure assumptions (Arakawa–Schubert and Fritsch–Chappell) and the Anthes-Kuo scheme. An additional sensitivity test was performed by comparing two different flux parameterization schemes over the ocean (Zeng and BATS).

There is a systematic underestimation of air temperature and precipitation when compared with analyzed data over the big domain area. Greater (~2 °C) and smaller (~0.9 °C) negative temperature biases are obtained in Grell–FC and Kuo convective scheme, respectively, and intermediate values are obtained in Grell–AS. The small domain simulation produces results substantially different, both for air temperature and precipitation. Temperature estimations are better for the small domain, while the precipitation estimations are better for the big domain.

An additional experiment showed that by using BATS to calculate the ocean fluxes in the big domain instead of the Zeng scheme, precipitation increases by 25% and the share of convective precipitation rose from 18% to 45% of the total, which implies a better simulation of precipitation. These changes were attributed to an increase of near surface latent heating when using BATS over the ocean. The use of BATS also reduces the cold bias by about 0.3–0.4 °C, associated with an increase of minimum temperature.

The behavior of the precipitation diurnal cycle and its relation with sea breeze was investigated in the small domain experiments. Results showed that the Grell–Arakawa–Schubert closure describes better this circulation as compared with Grell–Fritsch–Chappell closure.

1. Introduction

One of the main goals of regional climate models (RCMs) is to reproduce the main climatic features in complex terrain, where mesoscale forcing becomes important (Giorgi and Mearns, 1991) and coarse-resolution global climate models (GCMs) are not sufficient for assessing local climate change (Aldrian et al., 2004). An example of a region where present-generation GCMs are especially lacking in their ability to represent

complex terrain and land–sea contrasts is the Caribbean zone, where thousands of islands with a wide spectrum of extensions are surrounded by the Atlantic Ocean, the Caribbean Sea and the Gulf of Mexico, limited by the coasts of North and South America. In this region, tropical and extratropical systems interact (Alfonso and Naranjo, 1996) and frequently produce complex meteorological conditions. The sea-breeze circulation in islands and peninsulas favors the development of convective systems (Riehl, 1979). In such a complex meteorological situation, a high-resolution model is necessary for meaningful regional climate prediction.

Most previous applications and sensitivity studies using regional climate models have dealt with continental areas (Giorgi and Shields, 1999; Kato et al., 1999; Jenkins et al., 2002). It is only very recently that the first results have been obtained for the tropical archipelagos of Indonesia and the Philippines (Aldrian et al., 2004; Francisco et al., 2006). The main objective of the present paper is to test the performance of a regional climate model (RegCM3) in the Caribbean zone by evaluating its sensitivity to the convective parameterization scheme, domain size and resolution, and oceanic surface flux scheme. This study is particularly focused on model predictions for the biggest Caribbean islands, and mainly for Cuba. The simulated period is three months preceded by one month for spin-up of the model, from June 1993 to the end of September.

Section 2 provides a description of the model, data and numerical experiments used to investigate the RegCM3 performance. A brief description of the meteorological characteristics of the simulation period is presented in Sect. 3. Section 4 presents the simulation results for different convective schemes and domains, including sensitivity to ocean surface flux parameterization. Finally, Sect. 5 includes the summary and conclusions.

2. Model description, data and numerical experiments

2.1 Model description

The RegCM3 model (Elguindi et al., 2004) used in this study is an improved version of the RegCM2 (Giorgi et al., 1993a, b). It is a hydrostatic limited area model, with finite-difference discretization and a sigma coordinate in the vertical.

RegCM3 uses the radiation scheme of the NCAR CCM3 (Community Climate Model 3; Kiehl et al., 1996). The scheme calculates separately the heating and flux of solar and infrared radiation at the surface under conditions of clear and cloudy sky. The solar component follows the δ-Eddington approximation (Kiehl et al., 1996) and accounts for effect of CO_2, H_2O, O_3 and O_2. Cloud scattering and absorption parameterizations are also included. The infrared calculation accounts for effect of CO_2, H_2O and O_3 gases. The soil–vegetation–atmosphere interaction processes are parameterized using the Biosphere–Atmosphere Transfer Scheme (BATS), which is described in detail by Dickinson et al. (1993). BATS describes the role of vegetation and interactive soil moisture in modifying the surface-atmosphere exchanges of momentum, energy and water vapor. In the present version, 20 vegetation types are available. Each grid point of the model is represented by its dominant soil class and vegetation type, including the ocean surface as one of the soil classes.

Two parameterizations can be used in RegCM3 to represent the surface turbulent fluxes of momentum, heat and moisture over the ocean. One of them is BATS, implemented by Giorgi et al. (1993a, b), and the other is the one developed by Zeng (Zeng et al., 1998), which was implemented in RegCM3 (Elguindi et al., 2004).

In BATS, the near surface turbulent flux of moisture, heat and moment are calculated using a standard surface drag coefficient formulation based on surface-layer similarity theory. The drag coefficient depends on the atmospheric stability in the surface layer, as measured by the Richardson number, and on the surface roughness length. For BATS scheme the roughness length over the sea is constant and equal to 0.0004 m.

In the alternative Zeng scheme, the surface fluxes of momentum, heat and moisture also consider a drag coefficient-based bulk aerodynamic procedure. However, different of the BATS, the Zeng scheme considers the dependence of roughness length on the surface friction velocity. For momentum and heat (and also moisture) calculations the roughness length follows Smith (1988) and Brutsaert (1982), respectively. This formulation tends to produce lower evaporation rate over

warm tropical oceans when compared to BATS scheme (Zeng et al., 1998).

Turbulent transports of sensible heat, momentum and water vapor in the planetary boundary layer (PBL) over land and ocean are calculated using the scheme developed by Holtslag et al. (1990), which permits nonlocal transport in the convective boundary layer.

2.1.1 Convective schemes

The convective precipitation parameterizations used in this paper are the modified-Kuo (Anthes, 1977) and the Grell (1993) schemes. In the Grell (1993) scheme deep convective clouds are represented by an updraft and a downdraft that are undiluted and that mix with environmental air only in the base and top of the cloud. The heating and moistening profiles are derived from the latent heat release or absorption, linked with the updraft–downdraft fluxes and compensating motion. The Grell scheme convective closure assumption can be of two types. In the Arakawa–Schubert (1974) closure (GAS), a quasi-equilibrium condition is assumed between the generation of instability by grid-scale processes and the dissipation of instability by sub-grid (convective) processes. In the Fritsch–Chappell (GFC) closure (Fritsch and Chappell, 1980), the available buoyant energy is dissipated during a specified convective time period (between 30 min and 1 hour).

The Kuo scheme assumes that convection is started under conditions of convective instability and moisture convergence in the vertical column. Part of this moisture convergence precipitates and the rest is used to moisten the atmosphere. In the vertical a parabolic profile is used to distribute the latent heat of condensation, so that the maximum heating is located in the upper half of the cloud (Anthes, 1977).

2.1.2 Large-scale precipitation scheme

The large-scale precipitation scheme used in RegCM3 is described in Pal et al. (2000) and will be referred as SUBEX (subgrid explicit moisture scheme). This scheme considers the sub grid variability in clouds by linking the average grid cell relative humidity to cloud fraction and cloud water following the work of Sundqvist et al. (1989). SUBEX also includes the evaporation and accretion processes for stable precipitation.

2.2 The data sets

The initial and boundary conditions for RegCM3 were provided by NCEP–NCAR reanalysis (Kalnay et al., 1996). The reanalysis data set has a horizontal resolution of $2.5^\circ \times 2.5^\circ$ latitude by longitude, with a temporal resolution of 6 hours (00:00, 06:00, 12:00 and 18:00 UTC), and 17 pressure levels, from 1000 to 10 hPa. The variables used were geopotential height, air temperature, relative humidity, horizontal wind components and mean sea level pressure.

Sea surface temperature (SST) was obtained by interpolation of the monthly average values of the Reynolds and Smith (1994) data set. The topography and landuse data, derived from United States Geological Survey (USGS) and Global Land Cover Characterization (GLCC, Loveland et al., 2000), respectively, with horizontal resolution of 10-min, were used to provide the terrain characteristics.

The monthly climatology of air temperature and precipitation over the continents, except Antarctica, of the Climate Research Unit (CRU) of the University of East Anglia (New et al., 2000) was utilized to verify the RegCM3 results. This data set has horizontal resolution of $0.5^\circ \times 0.5^\circ$ longitude by latitude. The CPC Merged Analysis of Precipitation (CMAP), which is developed by the Climate Diagnostic Center (US Dept of Commerce) following the methodology of Xie and Arkin (1997), was also used for verification purposes. The CMAP analysis has the advantage that it provides precipitation estimates over the oceans. It should be noted that the CMAP horizontal resolution of $2.5^\circ \times 2.5^\circ$ longitude by latitude is too coarse to represent some of the fine-scale details predicted in our model, so that the CMAP data presented here should be used only to evaluate the larger-scale precipitation patterns. Additionally, the monthly means from the 65 stations of the Cuban surface network (CSN) were used to verify model output for Cuba.

2.3 Numerical experiments

Table 1 shows the general design of the simulations, accomplished to investigate the influence of the different factors in the performance of RegCM3. Two domains were used, whose

Table 1. General design parameters of the sensitivity experiments

Experiment	Domain	Horizontal resolution	Convective scheme	Closure	Terrain resolution	Surface flux over ocean
BGAS	Big	50 km	Grell	Arakawa–Schubert	10′	Zeng
BGFC	Big	50 km	Grell	Fritsch–Chappell	10′	Zeng
BKUO	Big	50 km	Kuo	–	10′	Zeng
BGASB	Big	50 km	Grell	Arakawa–Schubert	10′	BATS
SGAS	Small	25 km	Grell	Arakawa–Schubert	10′	Zeng
SGFC	Small	25 km	Grell	Fritsch–Chappell	10′	Zeng
SKUO	Small	25 km	Kuo	–	10′	Zeng
SGASB	Small	25 km	Grell	Arakawa–Schubert	10′	BATS

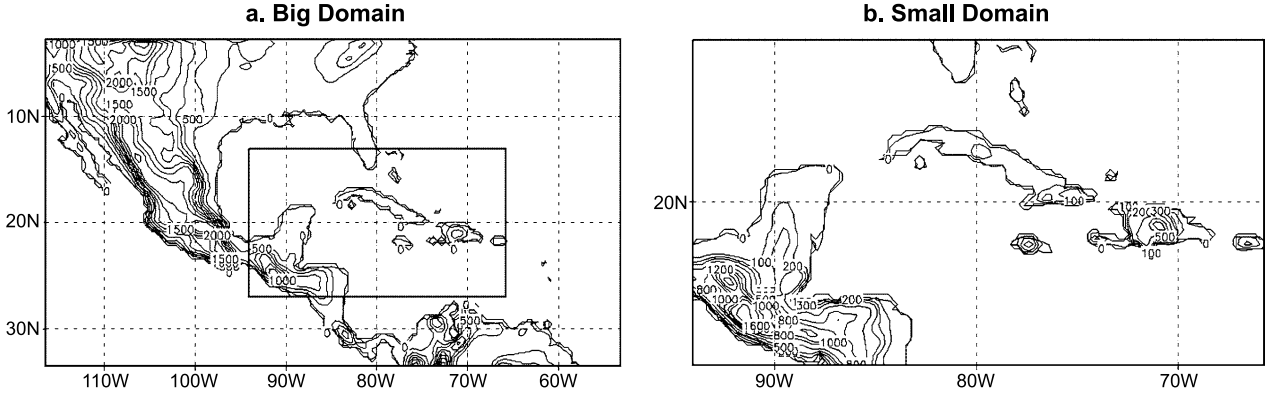

Fig. 1. The topography in the big (**a**) and small (**b**) domains. (Height contours are expressed in meters)

topography can be seen in Fig. 1 (a, b). The first, labeled as big domain, encompasses the whole Caribbean Region, including the Eastern and Western Antilles, Central America, Mexico, the southeastern USA and the northern coast of South America at a horizontal grid spacing of 50 km (78×144 grid points). The second one, labeled as small domain, was centered in Cuba, and encompasses the surrounding seas, including the Florida and Yucatan peninsulas, part of Central America and the islands of La Española and Jamaica, at a horizontal resolution of 25 km (69×129 grid points). In the vertical, the model considers 18 sigma levels with higher resolution in the boundary layer. In this set of experiments, the surface fluxes over the ocean were calculated using the Zeng scheme.

Additional sensitivity experiments were conducted focused on the influence of the surface flux over the ocean. This was done by changing the Zeng by BATS scheme, both in small and big domains, to represent the surface fluxes. This last experiment was performed only for the Arakawa–Schubert closure case.

The period of simulation extended from June to September 1993, which is part of the rainy season for the region. The initial conditions for RegCM3 experiments were set on 0000 UTC 01 June of 1993, and during the model integration the update of lateral boundaries is done every 6 hours. For initial and boundaries conditions the NCEP–NCAR reanalysis data set were used. The first month (June) of the simulations was considered as spin-up time and was excluded of the verification. For soil variables (water content at three soil layers) the initial condition is supplied by climatological values as function of the soil characteristics and at following times these variables are obtained by applying the BATS scheme over continental areas of domain.

The implicit type of averaging used in the analysis of the experimental results is continuous averaging of model output for the entire domain or some special areas, monthly or for the whole

experimental period, with the exception of the analysis of the diurnal cycles of surface wind and air temperature. For verification calculations, spatial averaging for specific regions is also used.

3. Meteorological characterization of the experimental period

The July–August period of 1993 was characterized by practically continuous influence of oceanic high-pressure zones, conditioning the inhibition of tropical waves over the 20° N parallel. In August, cyclonic activity intensified in the area, with the occurrence of five tropical storms (TS), all of which remained inside the Northwestern Atlantic with the exception of TS Bret, which moved into the Southern Caribbean Sea. In September there were three other TS, two of which remained in the Northwestern Atlantic with the third (hurricane Gert) crossing the Yucatan Peninsula into the Gulf of Mexico.

In Cuba, in July, most surface stations recorded rainfall under half of the historic average, temperature was higher than normal, and the ENSO influence was detected (Lapinel et al., 2002). August had a similar behavior, and the ENSO influence gradually diminished until the end of the month. In September, the rainfall regime was near to the norm, and one cold front passed through the Island, which is not a frequent event for this month.

4. Results and discussion

4.1 Large-scale features

Several simulations were made with the objective to assess the ability of the model to reproduce the typical circulation patterns and pressure fields of the Caribbean Region. There is no outstanding parameterization dependence in the capability to reproduce these features. All the tested combinations of physical parameterizations produced results consistent with the mean large-scale situations inferred from reanalysis. This is exemplified in Fig. 2, where the average sea level pressure field for July–September is shown for NCEP reanalysis and for the BGAS experiment (a, b; see Table 1 for the experiment names). The wind vector and specific humidity fields at 850 hPa are shown in Fig. 2c, d, and wind vector field at 200 hPa with wind intensity are shown in Fig. 2e, f. As expected, the large-scale fields are generally reproduced in more detail by RegCM3. For example, the subtropical anticyclone over North Atlantic and the thermal low over central USA are very well positioned by RegCM3. In particular, the increase in resolution in RegCM3 allows a high surface pressure center, and a collocated humidity minimum to appear inside the domain in the North Atlantic anticyclone, while these features seem to have been averaged out by the lower resolution reanalysis. A similar effect occurs in the thermal low over central North America, which decreases its minimum pressure by about 3 hPa in BGAS relative to the reanalysis.

The 850 hPa wind shows an intensification of the low level jet over the USA is also produced in BGAS (Fig. 2d) relative to the NCEP reanalysis (Fig. 2c). The low level easterly winds over the Caribbean Sea are very well simulated by RegCM3. The 850 hPa specific humidity simulated by BGAS (Fig. 2d) experiment is similar in spatial distribution to the NCEP–NCAR reanalysis (Fig. 2d) where higher values are found over eastern coast of the US, the central-western Caribbean and the equatorial Pacific, with some differences in absolute values. However, in the Caribbean Sea and in the Florida Strait the BGAS simulated humidity is higher than obtained from reanalysis, which may be related with the relatively high SST associated with the so called warm pools in these regions (Maul, 1977; Mitrani and Diaz, 2004). This is consistent with the averaged evapotranspiration simulated by BGAS, which has values higher than $150\,\mathrm{W/m^2}$ for the Caribbean and the northern coast of Cuba, including the Florida Strait (not shown). The 200 hPa wind field in BGAS (Fig. 2f) follows that of NCEP reanalysis (Fig. 2e) for most of the domain, indicating that the higher resolution information provided by the regional model does not have a great influence in the upper troposphere. However, over the Caribbean Sea, between the Greater Antilles and the Central and South America coasts, there is an extended belt of weak wind where the average wind direction of the reanalysis and BGAS are opposite. This is obtained also for the other convective parameterizations, and so it seems to be a general result of the finer resolution in RegCM3.

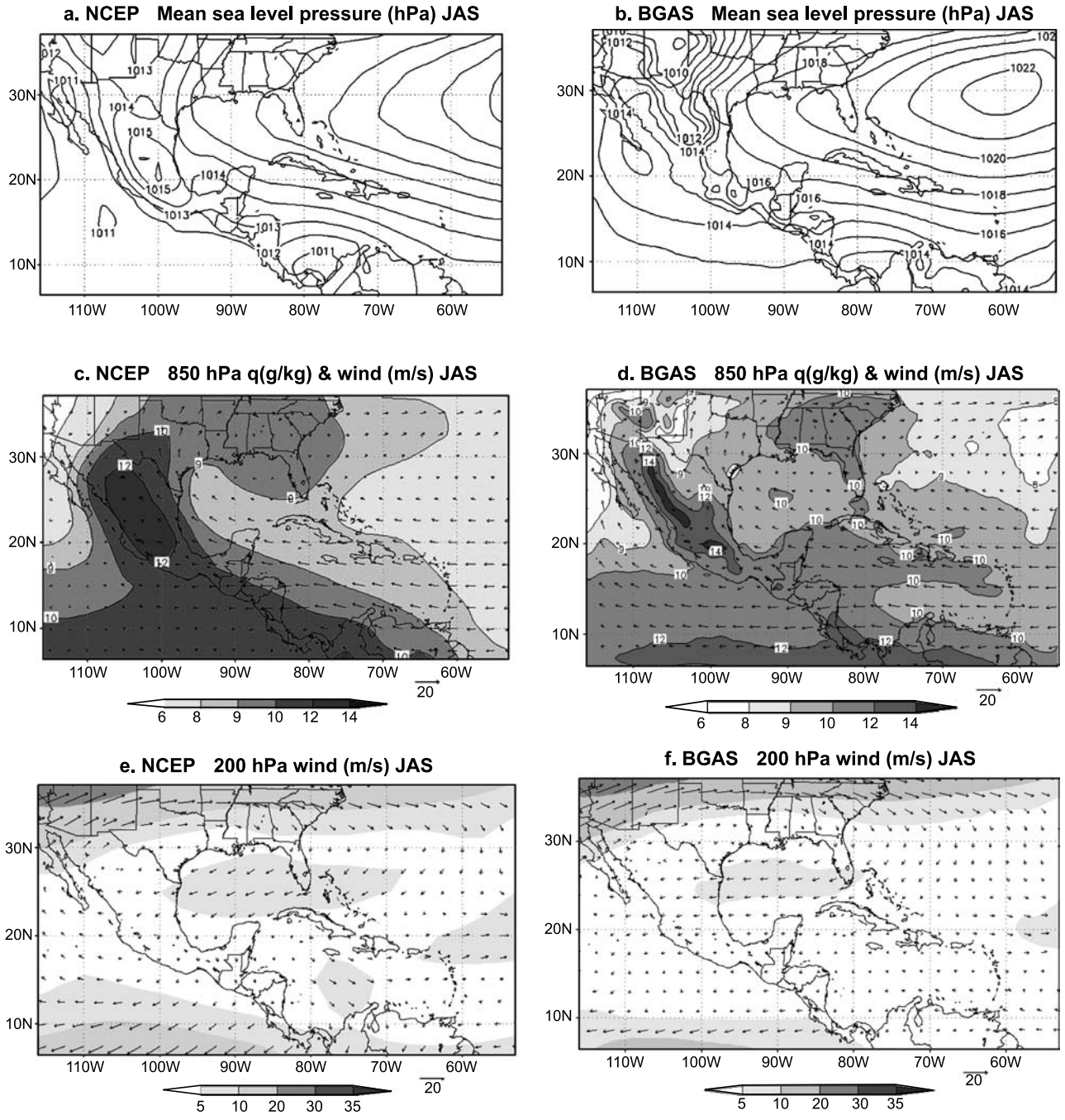

Fig. 2. Three month averaged plots (July–August–September 1993) of mean sea level pressure (hPa) field from NCEP–NCAR reanalysis (**a**) and from BGAS simulation (**b**); 850 hPa wind filed (arrows in m/s; scale at bottom) and specific humidity (in g/kg; shaded scale at the bottom) from NCEP–NCAR reanalysis (**c**) and from BGAS experiment (**d**); 200 hPa wind field (arrows and shaded in m/s, scale at bottom) from NCEP–NCAR reanalysis (**e**) and from BGAS experiment (**f**)

4.2 Sensitivity to convective parameterization scheme, domain size and resolution

4.2.1 Temperature and precipitation in the big domain

Over the ocean, the general pattern of near-surface temperature is well simulated in BGAS (Fig. 3a) and BKUO (Fig. 3b) compared with the CRU and reanalysis data, except over part of the Gulf Mexico, where simulated temperatures are lower than in the reanalysis (Fig. 4b). In BGFC the temperature over land and ocean was underestimated for almost all the domain. Over the mountain ridges, and the inland US, the ex-

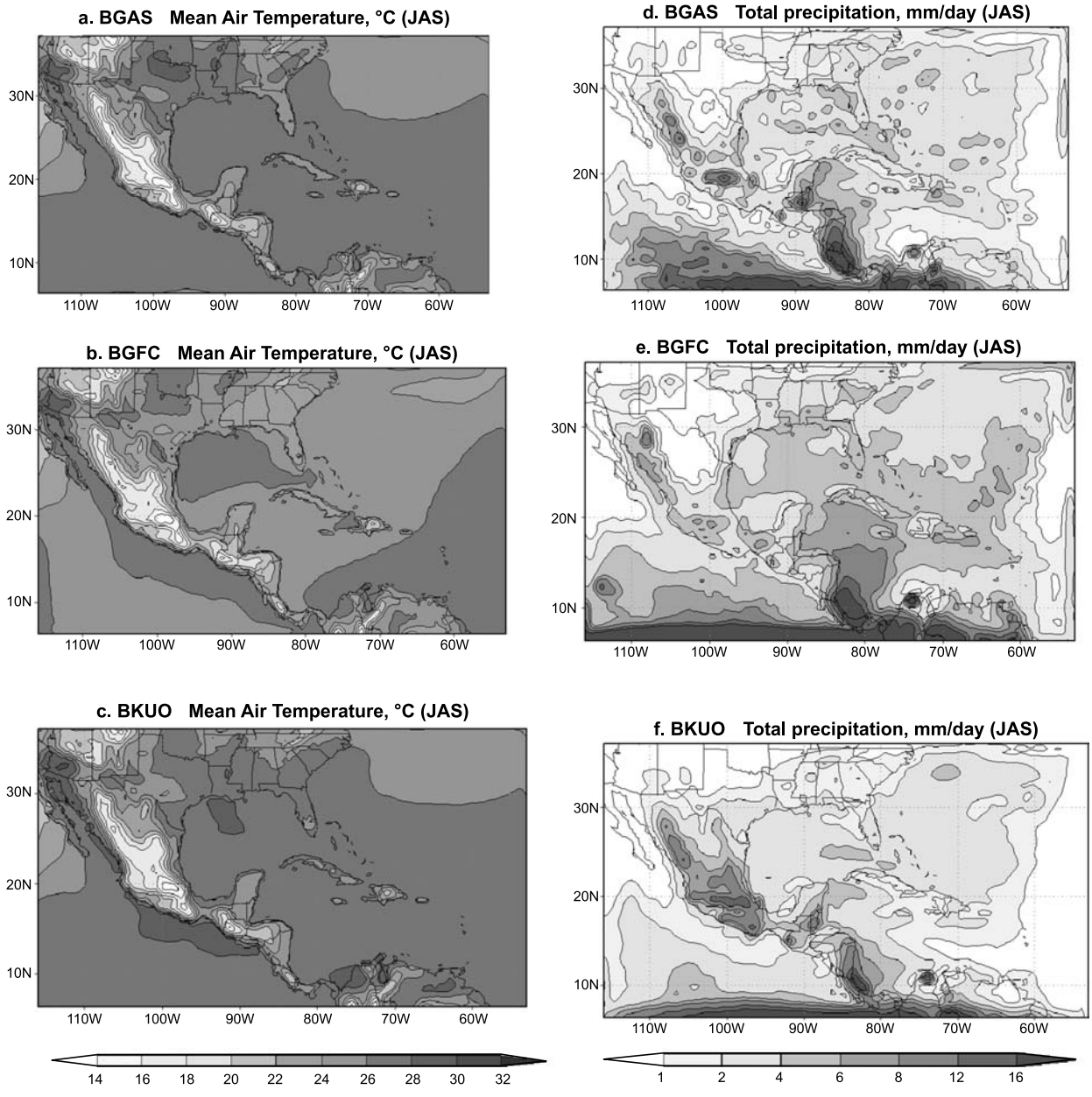

Fig. 3. July–August–September 1993 mean 2-m air temperature (**a**, **b**, **c**: shaded in °C) and total precipitation (**d**, **e**, **f**; shaded in mm/day) as simulated in the experiments BGAS (**a**, **d**), BGFC (**b**, **e**) and BKUO (**c**, **f**)

periments perform acceptably well. BKUO performs better regarding mean temperature over land, as the general pattern is well reproduced and the cold bias is much less apparent than in BGFC, except for the Yucatan peninsula and South Florida.

Precipitation over land is underestimated by BGFC (Figs. 3 and 4). This is evident for the western part of Mexico and California, Central America and the South of the United States. On the other hand, BGFC (Fig. 3e) overestimates precipitation over the southwestern Caribbean Sea, as compared with CMAP climatology (Fig. 4d). BGAS (Fig. 3d) reproduces the precipitation field better over part of Central America and western Mexico, and precipitation over the ocean in the southwestern Caribbean is not overestimated as in BGFC. For BKUO (Fig. 3f) the precipitation is concentrated over the continental areas, and is very low over the sea and the Greater Antilles as compared with the BGFC (Fig. 3e).

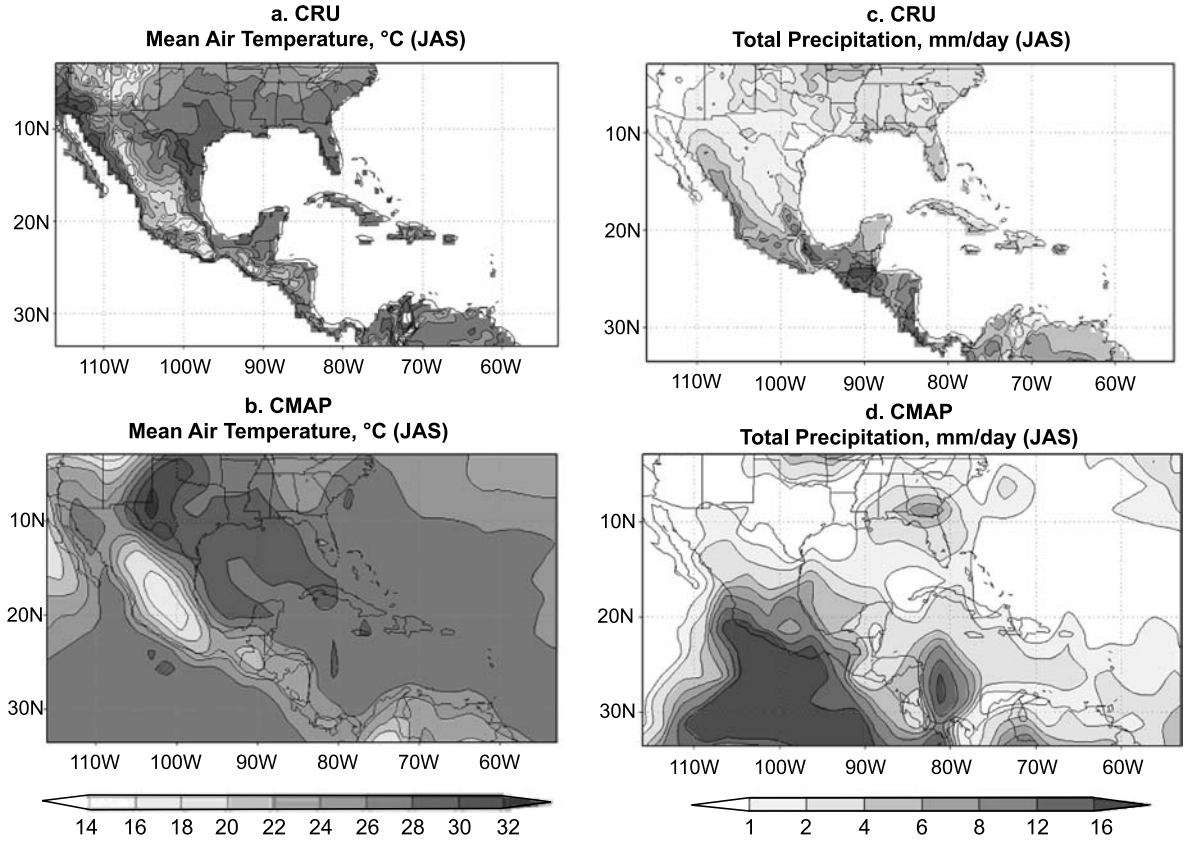

Fig. 4. July–August–September 1993 mean 2-m air temperature (**a**, **b**; shaded in °C) and total precipitation (**c**, **d**; shaded in mm/day) from CRU (**a**, **c**) and NCEP–NCAR (**b**, **d**) reanalysis

The model results were verified in comparison with CRU by calculating the average of the simulated values of air temperature and precipitation over the grid points of the CRU data. The verification was performed month-to-month and for seasonal climatology (Fig. 5). A cold temperature bias (Fig. 5a) was found in all cases, being smaller in BKUO and greater in BGFC. The observed temperature decrease in September was reproduced in the three experiments. The three simulations underestimate precipitation over land by roughly the same extent for the whole period. BKUO is the only one that reproduces the relative increase in precipitation during September, showing a physically plausible result as compared with the temperature decrease in the same month (Fig. 5a).

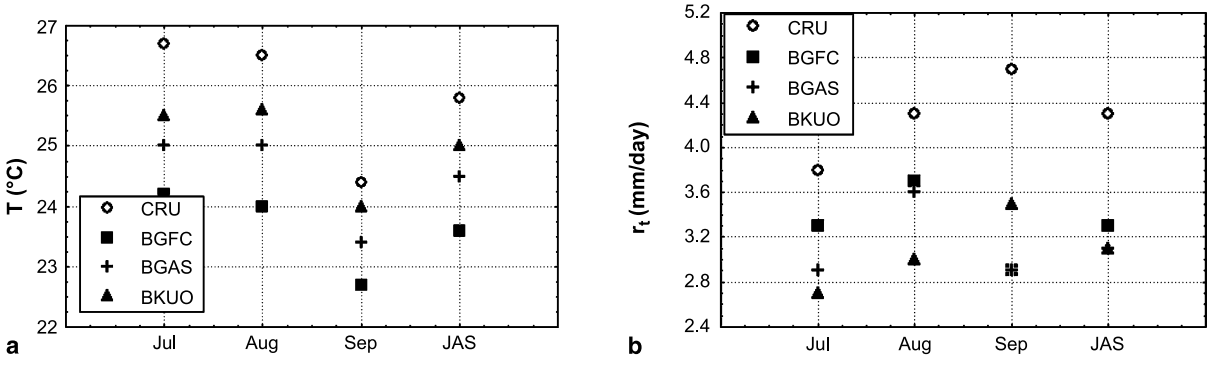

Fig. 5. Daily mean temperature (**a**), and daily total precipitation (**b**) averaged by month (July, August and September, 1993) and for the whole period (July–September, 1993), as estimated from CRU data and from BGFC, BGAS and BKUO simulations, for the Big Domain

Table 2. Average July–September 1993 radiation terms over the land areas of the big domain (W/m^2)

	SNet	INet	Id	S	LH	SH
BGAS	230	−68	384	272	−96	−58
BGFC	233	−68	381	275	−104	−56
BKUO	185	−52	402	219	−91	−47
BGASB	224	−63	391	265	−106	−60

SNet the net solar, *INet* the net infrared, *Id* the downward infrared, *S* the incident solar radiation, *LH* the latent heat and *SH* the sensible heat

To analyze the consistency of the cold bias and the precipitation deficit, which was observed in different degrees for the three simulations, the averaged radiation budget was calculated for the same grid points as the CRU data (Table 2). All radiation terms except the downward infrared are smallest in absolute magnitude for BKUO, while the simulated temperature for BKUO is higher than for the two Grell closures and the precipitation is roughly the same in the three cases. This is apparently contradictory, since less net radiation should produce lower surface temperature. However, different from the Kuo scheme, the Grell scheme includes a parameterization of downdrafts; apparently, the cooling associated with downdrafts may overwhelm the radiative effect to produce the cold bias in the BGFC and BGAS experiments. Figure 6a shows the area averaged temperature vertical profiles difference over land, obtained using the Kuo scheme and the two variants of the Grell parameterization. A temperature deficit is observed in both cases below the 6th σ level ($\sigma = 0.88$, approximately 900 hPa) which is consistent with downdraft cooling. In the middle troposphere, the BKUO experiment provided less heating, but in the higher levels, it is again warmer because of the absence of the cooling effect associated with overshooting cloud tops in the Grell scheme. The averaged profile of cloud water mixing ratio q_c over land (Fig. 6b) shows that, for the Kuo scheme, more cloud water is produced for all sigma levels over the 6th one and also the deepest layer with relatively high q_c is formed. The smaller net solar radiation in BKUO is probably a result of the enhanced cloudiness, consistent with BKUO having the greatest downward infrared and the smallest net infrared of all the experiments.

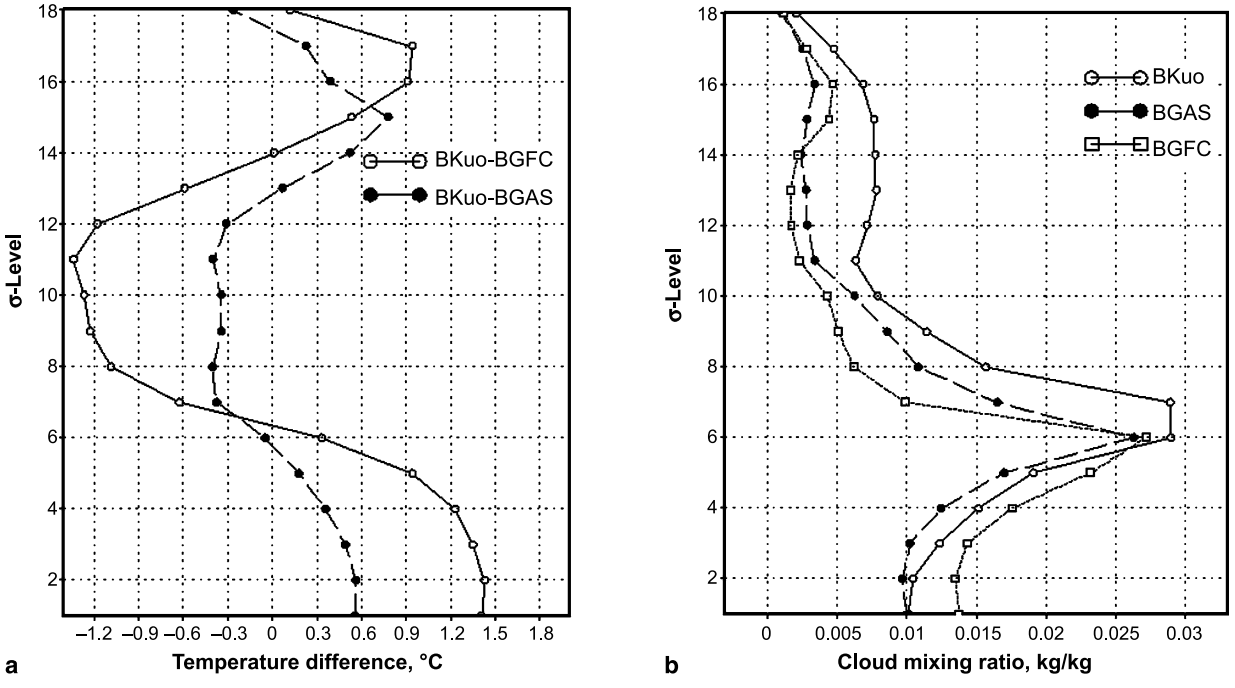

Fig. 6. Area averaged vertical profiles over land of (**a**) the difference between the mean air temperature estimation using the Kuo convective scheme and using the two variants of the Grell scheme (**b**) cloud mixing ratio obtained Kuo and the two Grell scheme simulations

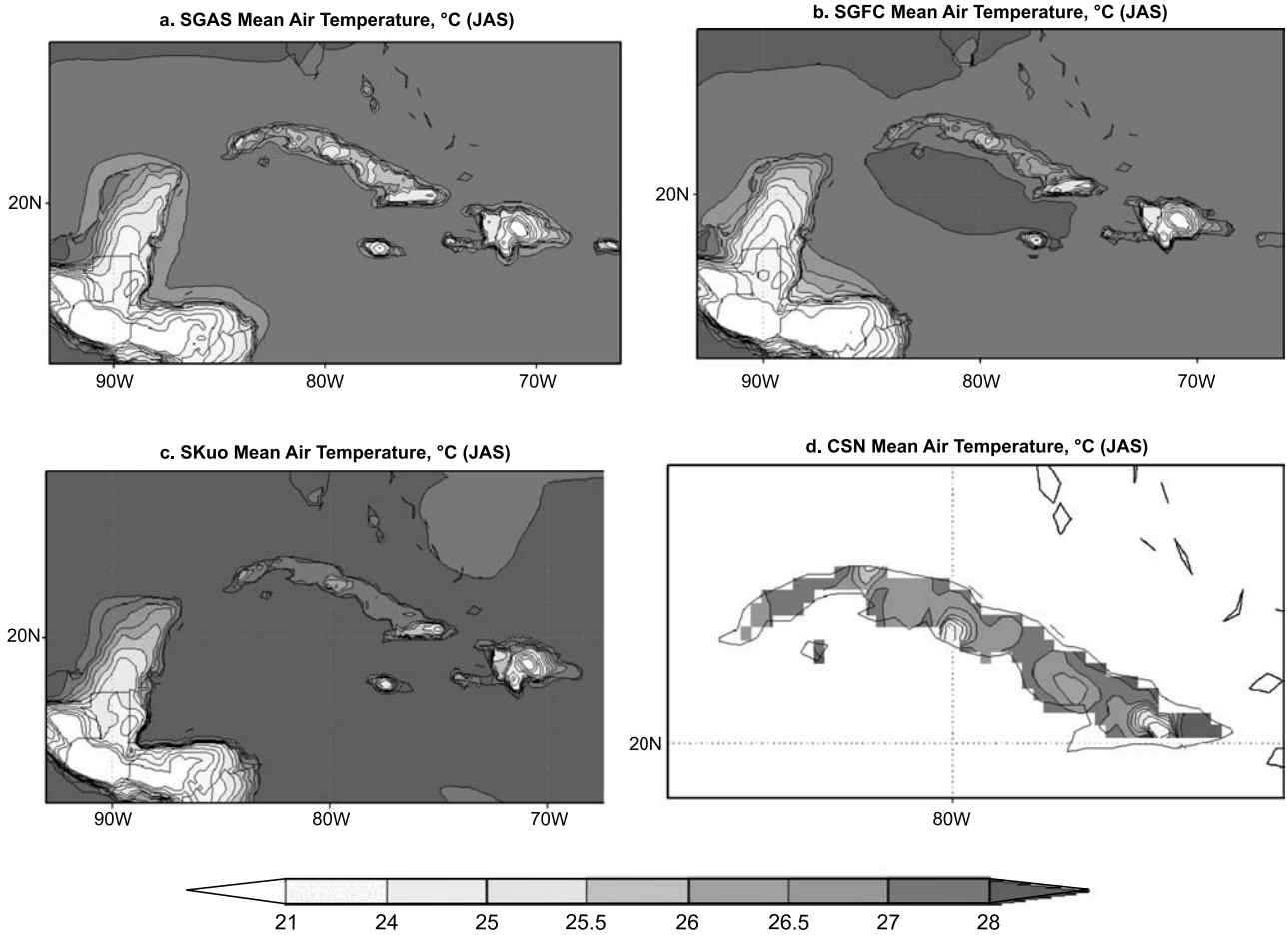

Fig. 7. July–August–September 1993 mean 2-m air temperature (shaded in °C) as simulated in the experiments SGAS (**a**), SGFC (**b**), SKUO (**c**) and observed by the Cuban Surface Network (CSN) (**d**)

4.2.2 Temperature and precipitation in the small domain

Figure 7 shows the air temperature spatial distribution for the simulations in the small domain for the three convective schemes and the CSN data. The simulations reproduce the main features of the measured surface temperature field over Cuba with the smaller temperatures over the elevated regions.

The general pattern of the precipitation field is also well reproduced by SGAS and SKUO (Fig. 7a, c). SGFC (Fig. 7b) performance is very poor for this domain, showing an excessive amount of precipitation over Cuba, compared to the Cuban surface network (Fig. 7d), CRU data (Fig. 4c) and also over the sea, as compared with CMAP data (Fig. 4d).

Comparison of simulated mean air temperature for the entire small domain with the CRU data (Fig. 9a) shows that in all simulations, mean air temperature is underestimated. SKUO is the best performing one, as its average bias for the whole period is only 0.5 °C. The two Grell simulations are very similar in this sense, and the under estimation in the mean temperature is greater than 1 °C. On the other hand, the precipitation bias (Fig. 9b) is less for SGFC, as the overestimation is about 1 mm/day, though with high spatial variability. The negative precipitation biases for the SKUO and SGAS experiments are nearly coincident and higher than 2 mm/day.

When compared with the CSN observations (Fig. 10a), the air temperature verification for Cuba shows that the results are not coincident with the above discussion regarding the entire small domain. The main differences that arise when the verification is restricted to Cuba are that SKUO produces a warm bias and that SGFC

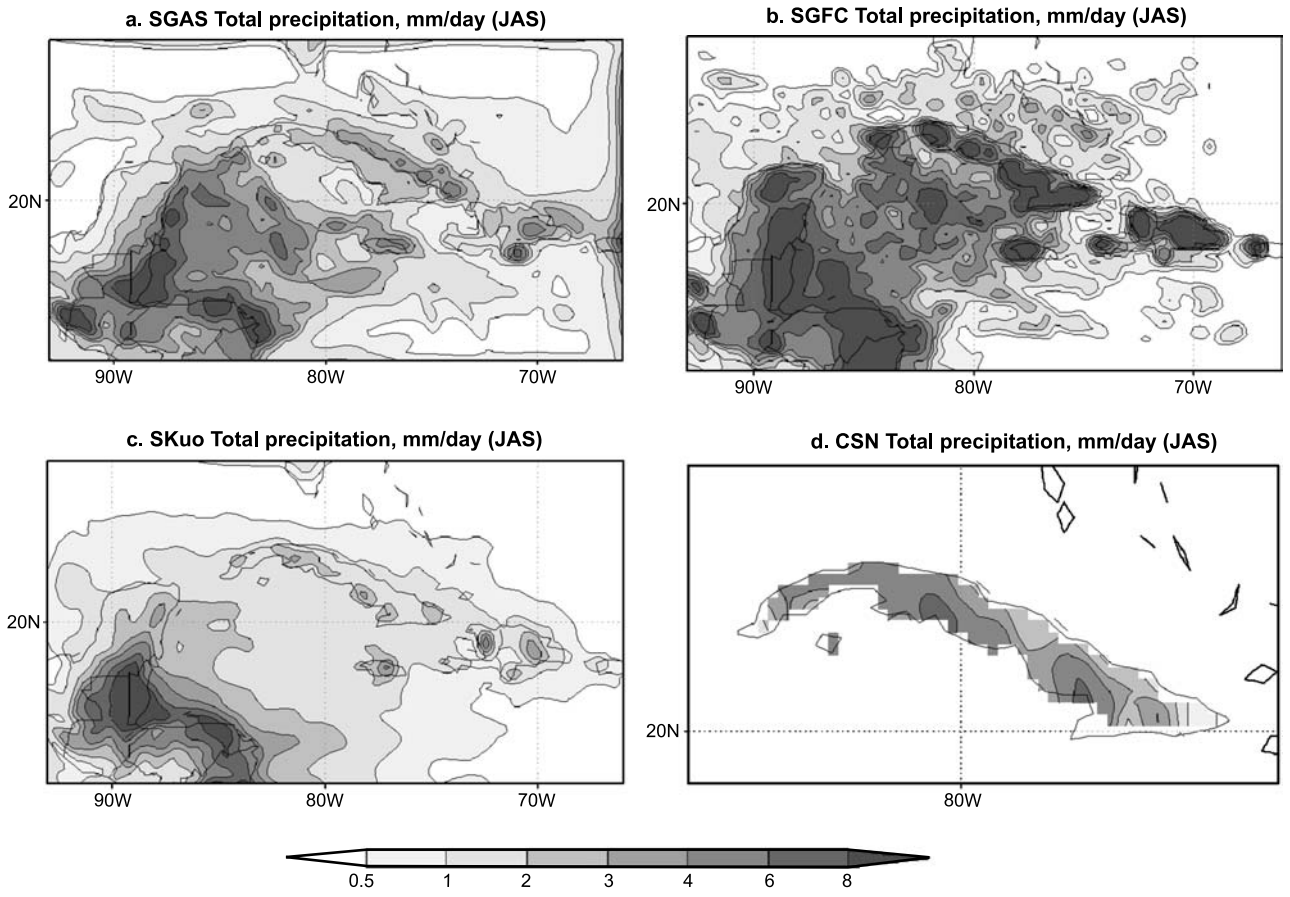

Fig. 8. July–August–September 1993 mean daily precipitation (shaded in mm day^{-1}) as simulated in the experiments SGAS (**a**), SGFC (**b**), SKUO (**c**) and observed by the Cuban network (**d**)

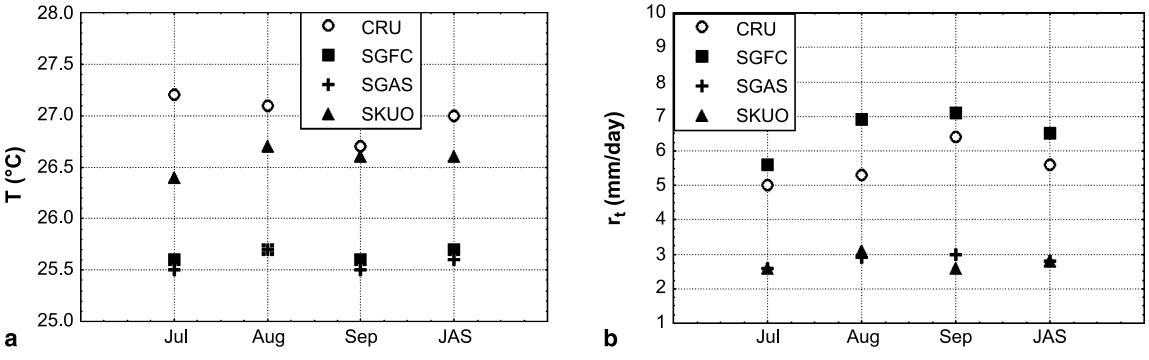

Fig. 9. Daily mean air temperature (**a**), and daily total precipitation (**b**) averaged by month (July, August and September, 1993) and for the whole period (July–September, 1993), as estimated from CRU data and from SGFC, SGAS and SKUO simulations, for the Small Domain

simulates well the air temperature. No relevant changes are noticed in precipitation for the island relative to the comparisons for the whole land portion of the small domain. The precipitation verification shows that the bias in SGAS is smaller month by month (Fig. 10b). SGFC better simulates the temperature over Cuba (Fig. 10a), as it produces nearly coincident values relative to CSN, while SKuo overestimates temperature in each month by 0.5–1 °C. SGFC overestimates precipitation during all the period, and greater precipitation is not associated to lower air tem-

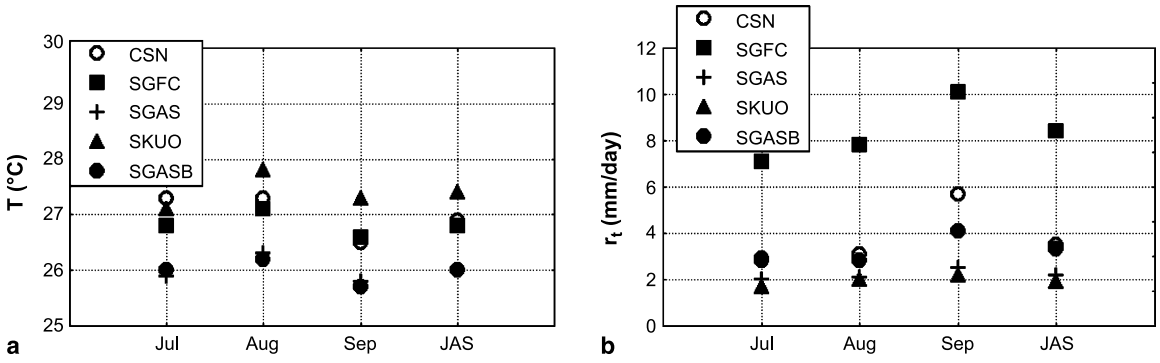

Fig. 10. Daily mean temperature (**a**), and daily total precipitation (**b**) averaged by month (July, August and September, 1993) and for the whole period (July–September, 1993), as estimated from Cuban surface network (CSN) data and from SGFC, SGAS and SKUO simulations, restricted to land areas of Cuba

perature. Month by month SKUO and SGAS simulate precipitation very close to CSN data, especially for July and August. For September both experiments underestimated precipitation by nearly 1 mm/day, and failed to predict the increase of precipitation in this month.

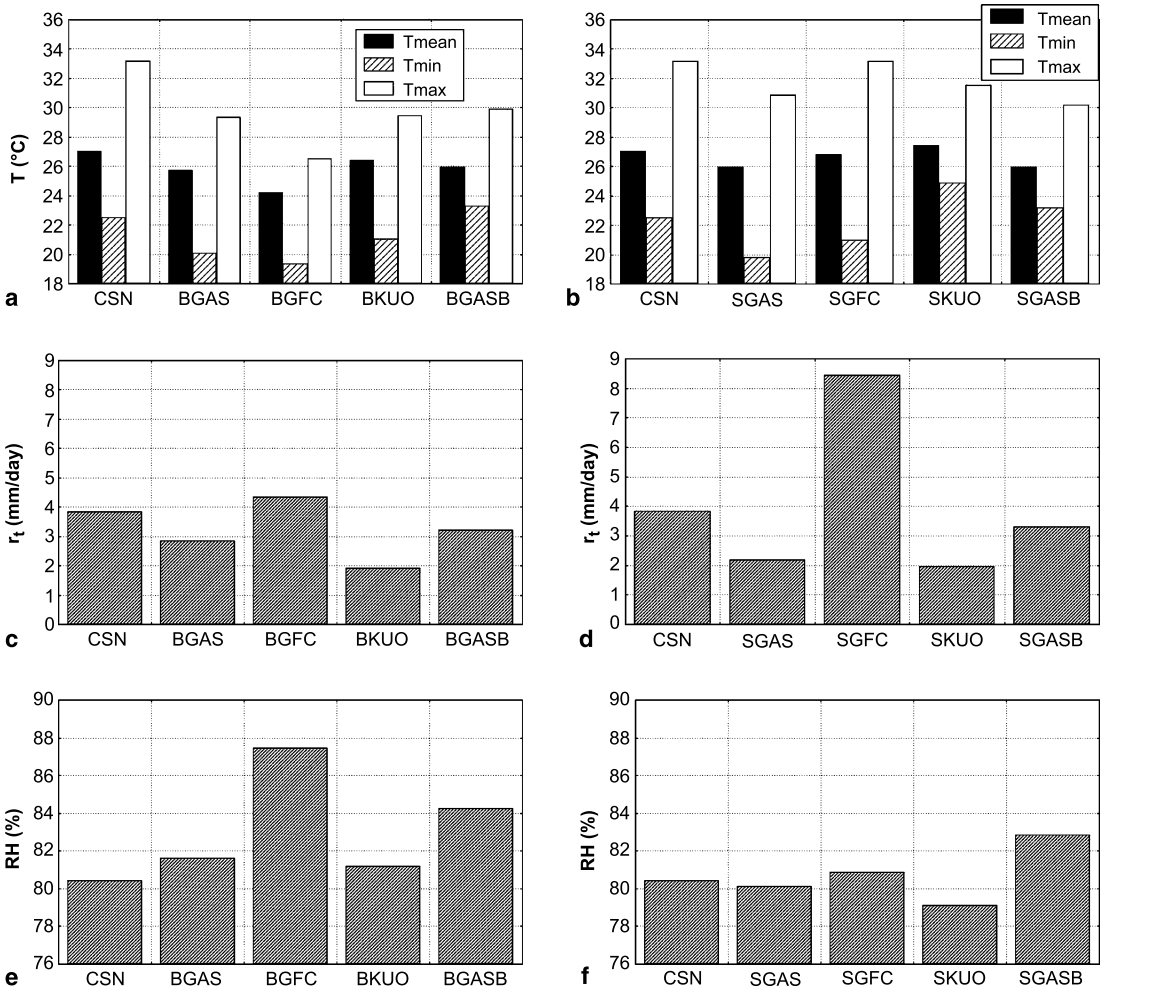

Fig. 11. Seasonal (JAS) averages of the meteorological variables for different experiments and for regridded CSN data over Cuba. (**a**, **b**) Air temperature (mean, maximum and minimum) for the big and the small domains. (**c**, **d**) Total precipitation for the big and small domains. (**e**, **f**) Relative humidity for the big and small domains

From the above discussion, it can be inferred that model results are sensitive to the change in domain in the Caribbean region. As Seth and Giorgi (1998) proposed, the domain of a regional climate model must be carefully selected for its specific application. To estimate this sensitivity, especially for Cuba, output from the big domain, small domain and CSN data were regridded and averaged over Cuba. Figure 11 shows the estimation of the seasonal (July–September) average of different meteorological variables for the Cuban territory, as produced by the various numerical experiments, for the big and the small domains. The CSN data were regridded for both domains for verification. The Grell–Fritsch–Chappell simulation is the most sensitive to domain size for all the variables. BKUO and SKUO produce acceptable estimations of maximum, minimum and mean temperature, but its estimations of maximum and minimum are visibly sensitive to domain size, including a change in bias sign. The temperature estimation in the Grell–Arakawa–Schubert case is the least sensitive to domain size. Regarding precipitation and relative humidity, neither the Kuo scheme nor the Grell–Arakawa–Schubert configurations are very sensitive to domain change over Cuba, but the GAS cases have the smallest biases. The three simulations have lower precipitation bias for the big domain. The use of high-resolution (2′) terrain data was tested and was found not to make a noticeable difference in the results.

4.3 Sensitivity to the ocean fluxes scheme

The model sensitivity to the ocean flux scheme was evaluated by using the Grell convective scheme with the Arakawa–Schubert closure in the big domain, as this parameterization proved not to be very sensitive to domain size change. Two additional experiments, denoted by BGASB and SGASB, were performed keeping all parameters as in BGAS and in SGAS, respectively, but changing the ocean flux algorithm from the Zeng to BATS scheme. The seasonal averages are remarkably similar between BGASB and SGASB for all the tested variables (Fig. 11), which is a sign of the robustness of this configuration of the model. This configuration has also the best or one of the best performances for the Cuban territory regarding the estimation of mean and minimum temperature and precipitation. For maximum temperature, SGFC performs better than the others in the small domain, but it gives the worst results for maximum temperature in the big domain, and heavily overestimates precipitation in the small domain. In the case of relative humidity, BGASB and SGASB perform worse than some of the other configurations for Cuba, but the absolute bias is small (3–4%).

Table 3. Mean values of convective and total precipitation (mm/day) over the BigDomain for BGAS and BGASB experiments

Experiment	Precipitation type	Jul.	Aug.	Sep.
BGAS	convective	0.54	0.69	0.61
	total	3.20	3.75	3.36
BGASB	convective	1.75	2.03	1.94
	total	4.00	4.60	4.40

Table 3 presents the monthly total and convective precipitation for BGAS and BGASB experiments. For the three months considered, the total precipitation in the BGASB experiment is higher by about 25% than for BGAS (Table 3). The partition between convective and non-convective precipitation is radically different between the two experiments. While in the BGAS the convective precipitation represents only about 18% of the total, in the BGASB it represents approximately 45%. This indicates that, by using the

Table 4. Month to month absolute and relative differences (values in parenthesis) of the near surface variables between BGASB and BGAS (BGASB–BGAS) experiments, calculated for the big domain

Variable	Jul.	Aug.	Sep.
Air temperature (°C)	0.46	0.45	0.53
Specific humidity (g/kg)	0.64 (+3.6%)	0.68 (+3.8%)	0.64 (+4.5%)
Sensible heat (W/m^2)	0.65 (2.3%)	0.89 (+3.1%)	1.42 (+5.2%)
Latent heat (W/m^2)	0.42 (+9.5%)	0.46 (+10.3%)	0.55 (+12%)
Net solar radiation (W/m^2)	−5.1 (−2.1%)	−4.2 (−1.8%)	−5.2 (−2.4%)
Net infrared radiation (W/m^2)	−3.53 (−6.3%)	−3.51 (−6.3%)	−3.90 (−6.8%)
Total rain (mm/day)	0.74 (+18%)	0.84 (+18%)	1.00 (+23%)
Convective rain	1.20 (+68%)	1.34 (+66%)	1.33 (+69%)

BATS scheme, the boundary layer develops meteorological profiles more favorable to deep convection. To clarify the reason for this behavior, the relative increase(+)/decrease(−) of some near surface variables are presented in Table 4 and discussed below. This relative difference for any variable X was calculated as:

$$\overline{X}\% = \frac{\overline{X}_{\mathrm{BGASB}} - \overline{X}_{\mathrm{BGAS}}}{\overline{X}_{\mathrm{BGAS}}}$$

where the over bar indicate the mean over big domain. The average difference between the two simulations considered all grid points in the big domain.

Both net solar and net infrared radiation terms decrease in BGASB. However, the relative decrease is greater for the net infrared radiation ($\sim -6.3\%$) than for the net solar radiation ($\sim -2\%$). This means that in BGASB the infrared radiative loss is smaller and contributes to higher ($\sim$0.5 °C) temperatures. BGASB produces a significant increase in the surface latent heat flux (about 10%) and this likely explains the increases in both the total rain and the fraction of convective rain simulated in this experiment. Increased sensible heating (about 2–5%) leads to higher air temperature (about +0.5 °C) in BGASB. The increase of both temperature and specific humidity produces an increase in moist static energy (cp T + gz + Lq) and so favors greater convective activity in the BGASB experiment (Table 3).

The positive impact of the BATS scheme in the simulations is presented in Table 5, showing the mean values over the big domain as calculated for CRU data and for experiments BGAS and BGASB. During each month considered and also for the season (JAS), the BGASB consistently shows a reduction of about 0.4 °C, relative to the cold bias produced by BGAS. Except for July, the reduction of the cold bias in BGASB experiment is accompanied by an increase of the monthly precipitation and this reduces the underestimation of the precipitation produced by the BGAS experiment.

Table 5. Average air temperature (°C) and precipitation (mm/day) over big domain for CRU data and the simulations BGAS and BGASB

	Air temperature (°C)			Precipitation (mm/day)		
	CRU	BGAS	BGASB	CRU	BGAS	BGASB
July	27.1	25.9	26.3	2.7	2.9	3.9
August	27.2	26.0	26.4	3.7	2.7	3.5
September	26.7	25.9	26.3	5.0	3.4	4.8
JAS	27.0	26.0	26.3	3.8	3.0	4.1

4.4 Regional circulation

Sea-breeze circulation is a main feature in local wind circulation in the islands (Riehl, 1979). Its relation with the thermal contrast between the coastline and the sea implies a marked diurnal cycle, which is related with the diurnal precipitation cycle as sea-breeze convergence acts as a trigger and organization factor in the formation of convective systems. In Cuba, the formation of convergence lines along some parts of the Island is a climatological feature, with its location dependent on large scale wind direction (Rivero and Medvedev, 1987; Beliaev et al., 1989). In this area, as the sea-breeze develops in the morning when the land surface becomes warmer than the sea, there is a tendency of the predominant low level east wind to decelerate. For this reason, the vector difference in surface wind between 07:00 LST in the morning (12 UTC) to 13:00 LST in the afternoon (18 UTC) can be taken as an approximation of the sea-breeze contribution to the surface wind field.

Figure 12 shows the average of this vector field for the month of July as obtained from SGAS and SGFC. Both experiments simulate almost equally well the formation of a line of convergence along the island and near to its central 'axis'. The corresponding averaged precipitation diurnal cycle for each of the two experiments are presented in the same figure. For SGAS, from 06 to 12 UTC precipitation develops mainly off shore, while from 18 UTC to 00 UTC a great deal of precipitation accumulates over land, as should be expected from the triggering effect of sea-breeze along the line of convergence. At night (06 UTC), precipitation decreases again. SGFC also predicts precipitation development over land during the afternoon (00 UTC), but this precipitation persists during the night (06 UTC), so that an unrealistic diurnal cycle occurs which contradicts observational evidence (Alvarez et al., 2002a, b). Contours in Fig. 13 show the simulated seasonally averaged

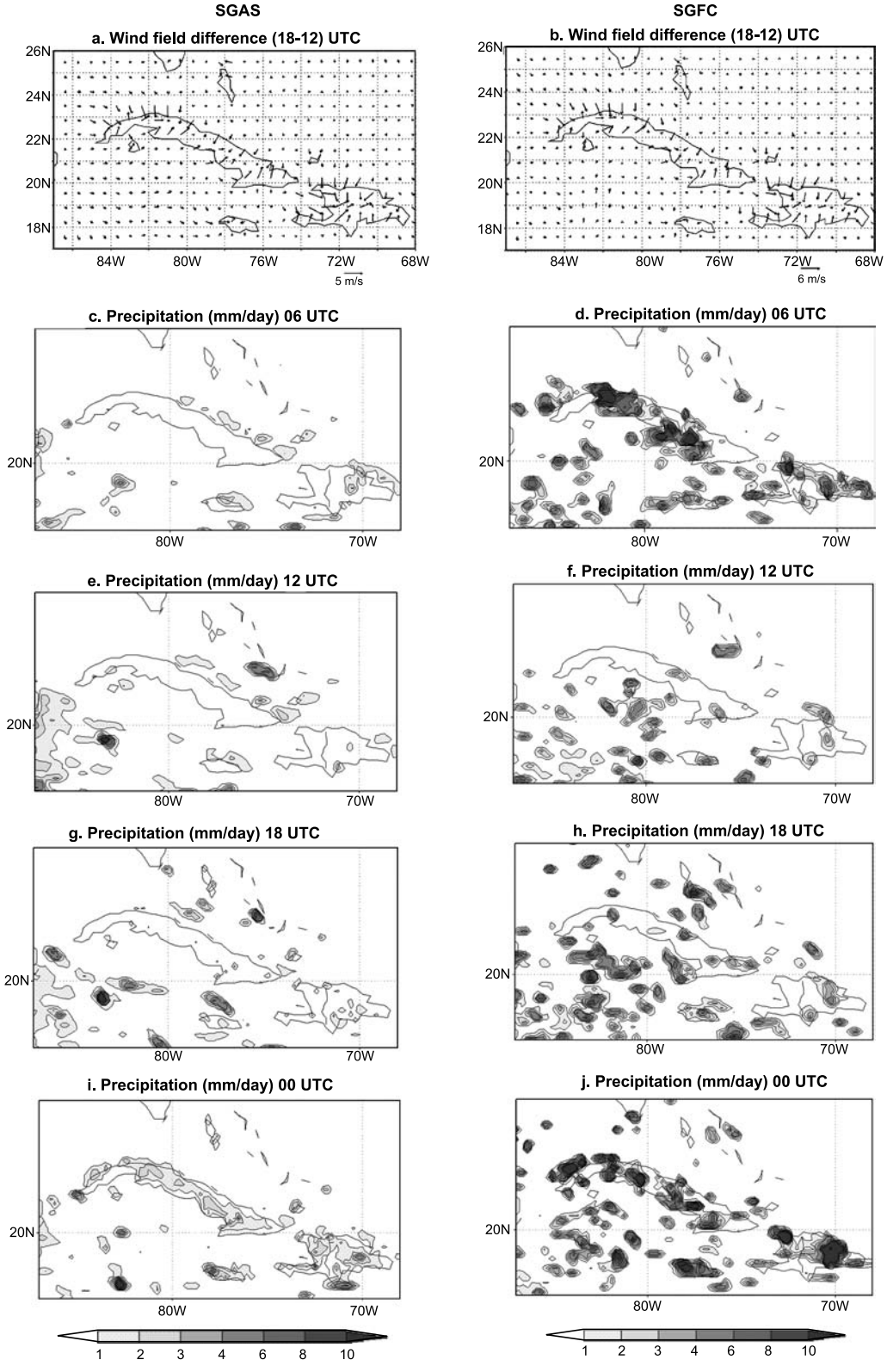

Fig. 12. Averaged vectorial difference between the wind fields at 18 UTC and 12 UTC for the region of Cuba and La Española, for the experiments SGAS (left column) and SGFC (right column) (**a**, **b**) and the diurnal evolution of the simulated precipitation rate (**c–j**). Averaged 6 hours cumulative precipitation, for four output times (00, 06, 12 and 18 UTC) for the month of July are shown in shaded contours

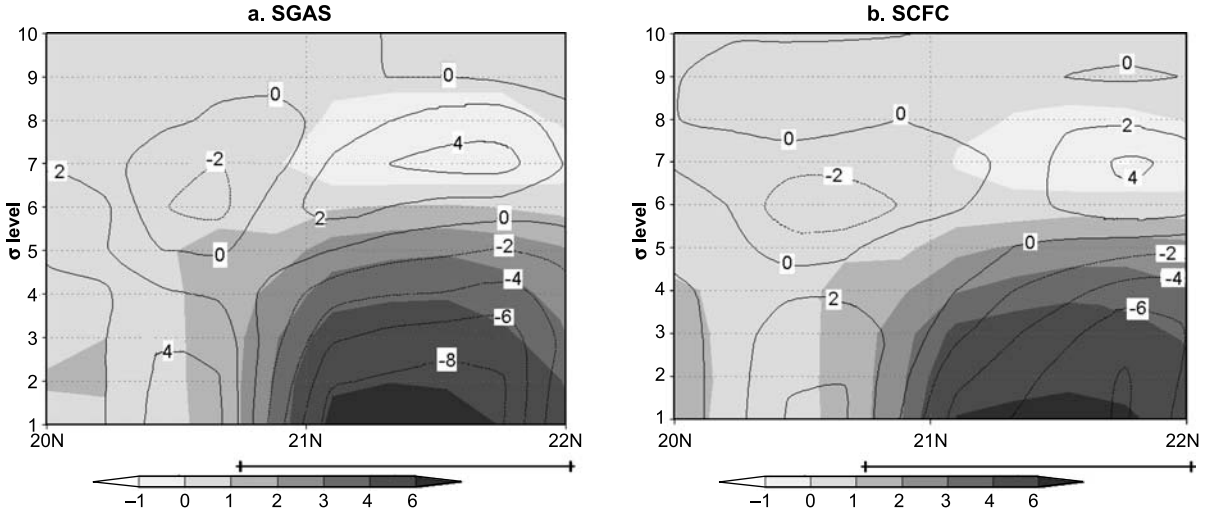

Fig. 13. Vertical cross sections along 78° W of the averaged difference between horizontal divergence (contours in $10^{-5}\,s^{-1}$) and temperature (shaded in K) at 18 and 12 UTC for SGAS (**a**) and SGFC (**b**). The line segment at the bottom of the figure indicates the land area of the Island of Cuba

vertical structure of wind divergence, associated with sea-breeze circulation, obtained from the difference between the divergence at 18 UTC and at 12 UTC in a sigma vertical cross section at constant longitude of 78° W, passing through the Cuban province of Camagüey, which is an almost flat territory, where the orographic factor is negligible. The averaged temperature difference at 18 UTC and 12 UTC is also shown. Figure 13a and b correspond, respectively to the SGAS and the SGFC experiments.

As can be seen, both experiments simulated a sea-breeze convergence maximum near the center of the Island, but for the SGAS, it was more intense and the convergence cell was wider and deeper. The sea-breeze convergence isolines for SGAS were also better collocated with the isolines of the average increase of temperature. This behavior is consistent with the greater ability of SGAS (left column of Fig. 12) compared to SGFC (right of Fig. 12) to simulate the diurnal precipitation cycle in Cuba.

5. Summary and conclusions

Performance of the RegCM3 model has been evaluated for a three-month summer period in two domains in the Caribbean region, using three different cumulus parameterization schemes and two ocean flux schemes. The applied cumulus parameterizations were the Grell scheme with the Arakawa–Schubert and the Fritsch–Chappell closure assumptions, and the Anthes-Kuo scheme. The effect of each parameterization was tested for two domains, a larger one, labeled as big domain, and a smaller one, labeled as small domain. In these experiments, the Zeng ocean flux scheme was used.

In the big domain, both the Grell scheme with Arakawa–Schubert closure (BGAS) and the Kuo scheme (BKUO) simulate well the general pattern, but the BGAS produces a cold bias for the islands and peninsulas. The Grell scheme with Fritsch–Chappell closure produces a cold bias in the whole big domain, and especially in the islands and peninsulas. The Grell parameterization produces a deficit of precipitation over land, and a surplus over the ocean that is more pronounced in the BGFC experiment. On the other hand, the BKUO experiment underestimates precipitation both over the ocean and land.

For the small domain, the general patterns of the air temperature and the precipitation fields are better reproduced than for the big domain. Verification over the land areas of the whole small domain using CRU data shows a reduction of the cold bias if compared to the big domain, though a cold bias persists, mainly for the Grell experiments. In SGAS and SKUO, precipitation is underestimated by more than 2 mm/day, while SGFC gives an overestimation of $\sim$1 mm/day. An additional verification was made using the high resolution Cuban Surface Network (CSN). The SGFC scheme provides the best simulation

of averaged air temperature relative to the CSN observations, while the SGAS and SKuo are the best simulation of CSN precipitation.

As a result of the comparison of the big domain and small domain experiments in the same grid points over land, relative to the CRU data, it can be concluded that the temperature estimations are better for the small domain, while the precipitation estimations are better for the big domain. The least sensitive parameterization regarding change of domain and model resolution was the Grell–Arakawa–Schubert, so that it was chosen to accomplish the test of sensitivity to the ocean flux scheme change. To do this, an additional experiment was made in the big domain, using BATS (BGASB) to calculate the ocean fluxes. In this case, precipitation was increased by 25%, and the share of convective precipitation rose from 18% to 45% of the total. This is related to increases of 10% for latent heat flux and 2–5% for sensible heat flux.

The relation between sea-breeze circulation and the precipitation diurnal cycle in Cuba and La Española was exemplified by means of a one-month experiment, using the two closures of the Grell scheme. A clear averaged sea-breeze convergence line near the longitudinal centers of the two islands was obtained from the two experiments at 18 UTC. However, a more realistic diurnal precipitation cycle was obtained with the Grell–AS than with the Grell–FC closure scheme. While the circulation over Cuba is realistic, the grid spacing of 25 km may be too coarse to resolve the sea breeze over some of the smaller islands. This could perhaps be a partial explanation for some of the errors in the precipitation field.

Comparing all experiments, and especially from the analysis of the geographical distribution of precipitation for the Grell–AS and the Grell–FC schemes, it can be concluded that the AS closure leads to a more consistent pattern of temperature and precipitation distribution for the region, even if the FC experiments give good estimations of average temperature over land. The Kuo scheme performed acceptably well for both domains, and can be used for long term area-averaged climatology, but from its physical assumptions it has well known limitations to reproduce the diurnal cycle of precipitation and so to study the effects of local mesoscale systems.

Acknowledgments

We thank the Weather and Climate Physics Group of the International Centre for Theoretical Physics for providing the RegCM3 model and for managing the RegCNet international collaboration network. We specially acknowledge the useful suggestions of Filippo Giorgi and Jeremy Pal and the detailed revision of Lisa Sloan and two unknown reviewers.

References

Aldrian E, Dümenil-Gates L, Jacob D, Podzun R, Gunawan D (2004) Long-term simulation of Indonesian rainfall with the MPI regional model. Clim Dyn 22: 795–814

Alfonso AP, Naranjo LR (1996) The 13 March 1993 severe squall line over Western Cuba. Wea Forecasting 11: 89–102

Alvarez L, Alvarez R, Borrajero I (2002) Caracterización de las precipitaciones en la estación meteorológica de Casablanca y su tendencia. Rev Cub Meteor 9(1): 61–70

Alvarez L, Alvarez R, Borrajero I, Iraola C (2002) Caracterización de las precipitaciones en la estación meteorológica de Camagüey y su tendencia. Rev Cub Meteor 9(2): 28–37

Anthes RA (1977) A cumulus parameterization scheme utilizing a one-dimensional cloud model. Mon Wea Rev 105: 270–286

Arakawa A, Schubert WH (1974) Interaction of a cumulus cloud ensemble with the large scale environment. Part I. J Atmos Sci 31: 674–701

Beliaev V, Valdés M, Martínez D, Petrov V (1989) An airborn study of the structure of cloud bands observed over the Camagüey Meteorological Site. Trudy TsAO, 172: 11–16. (In Russian. Spanish version available at the Center for Atmospheric Physics. INSMET, Cuba)

Brutsaert W (1982) Evaporation into the atmosphere: theory, history and applications. USA: Reidel Himgham Mass, 299 pp

Dickinson RE, Henderson-Sellers A, Kennedy PJ (1993) Biosphere-atmosphere transfer scheme (BATS) version 1E as coupled to the NCAR Community Climate Model. Boulder, Colorado: Tech Note NCAR/TN-387, 72 pp

Elguindi N, Bi X, Giorgi F, Nagarajan B, Pal J, Solmon F (2004) RegCM Version 3.0 User's Guide. Trieste: PWCG Abdus Salam ICTP, 48 pp

Francisco RV, Argete J, Giorgi F, Pal J, Bi X, Gutowski W (2006) Regional model simulation of summer rainfall over the Philippines: effect of choice of driving fields and ocean flux schemes. Theor Appl Climatol (in this issue)

Fritsch JM, Chappell CF (1980) Numerical prediction of convectively driven mesoscale pressure systems. Part I: Convective parameterization. J Atmos Sci 37: 722–1733

Giorgi F, Marinucci MR, Bates GT (1993a) Development of a second generation regional climate model (RegCM2). Part I: Boundary layer and radiative transfer processes. Mon Wea Rev 121: 2794–2813

Giorgi F, Marinucci MR, Bates GT, De Canio G (1993b) Development of a second generation regional climate model (RegCM2). Part II: Convective processes and assimilation of lateral boundary conditions. Mon Wea Rev 121: 2814–2832

Giorgi F, Mearns LO (1991) Approaches to regional climate change simulation: a review. Rev Geophys 29: 191–216

Giorgi F, Shields C (1999) Tests of precipitation parameterizations available in the latest version of the NCAR Regional Climate Model (RegCM) over the continental United States. J Geophys Res 104: 6353–6375

Grell GA (1993) Prognostic evaluation of assumptions used by cumulus parameterizations. Mon Wea Rev 121: 764–787

Holtslag A, De Bruijn E, Pan H-L (1990) A high resolution air mass transformation model for short-range weather forecasting. Mon Wea Rev 118: 1561–1575

Jenkins GS, Kamga A, Garba A, Diedhiou A, Morris V, Joseph E (2002) Investigating the West African climate system using global/regional climate models. Bull Amer Meteor Soc 83: 583–595

Kalnay E et al. (1996) The NCEP/NCAR 40-Year Reanalysis Project. Bull Amer Meteor Soc 77: 437–471

Kato H, Hirakushi H, Nishizawa K, Giorgi F (1999) Performance of NCAR RegCM in the simulation of June and January climates over eastern Asia and the high-resolution effect of the model. J Geophys Res 104: 6455–6476

Kiehl JT, Hack JJ, Bonan GB, Boville BA, Briegleb BP, Williamson DL, Rasch PJ (1996) Description of the NCAR Community Climate Model (CCM3). Boulder, Colorado: Tech. Note, NCAR/TN-420 + STR, 152 pp

Lapinel B, Pérez D, Cutié V, Fonseca C (2002) Los eventos ENOS y su asociación con la sequía en Cuba. Rev Cub Meteor 9(2): 38–48

Loveland TR, Reed BC, Brown JF, Ohlen DO, Zhu J, Yang L, Merchant JW (2000) Development of a global land cover characteristics database and IGBP DISCover from 1-km AVHRR Data. Int J Remote Sensing 21: 1303–1330

Maul GA (1977) On the annual cycle of the Gulf Loop Current: Part 1: observations during a one-year time series. J Marine Research 35: 29–47

Mitrani I, Díaz OO (2004) Relationship between the thermal vertical structure of Cuban waters and tropical cyclone activity. Ciencias Marinas 30: 335–341

New M, Hulme M, Jones P (2000) Representing twentieth-century space-time climate variability: Part II: Development of 1901–1996 monthly grids of terrestrial surface climate. J Climate 13: 2217–2238

Pal JS, Small EE, Elthair EA (2000) Simulation of regional-scale water and energy budgets: representation of subgrid cloud and precipitation processes within RegCM. J Geophys Res 105: 29579–29594

Reynolds RW, Smith TM (1994) Improved global sea surface temperature analysis using optimum interpolation. J Climate 7: 929–948

Riehl H (1979) Climate and weather in the tropics. London: Academic Press, 595 pp

Rivero R, Medvedev GA (1987) Regional features of the development of convective clouds and precipitations in the Central part of the Island of Cuba. In: Tropical meteorology. Leningrad, Gidrometeoizdat: Proceedings of the Third International Simposium, 245–353. (In Russian. Spanish version available at the Center for Atmospheric Physics. INSMET, Cuba)

Seth A, Giorgi F (1998) The effects of domain choice on summer precipitation simulation and sensitivity in a regional climate model. J Climate 11: 2698–2712

Smith SD (1988) Coefficients for sea surface wind stress, heat flux, and wind profiles as a function of wind speed and temperature. J Geophys Res 93: 15467–15472

Sundqvist HE, Berge E, Kristjansson JE (1989) The effects of domain choice on summer precipitation simulation and sensitivity in a regional climate model. J Climate 11: 2698–2712

Xie P, Arkin PA (1997) Global precipitation: a 17-year monthly analysis based on gauge observations, satellite estimates, and numerical model outputs. Bull Amer Meteor Soc 78: 2539–2558

Zeng X, Zhao M, Dickinson RE (1998) Intercomparison of bulk aerodynamic algorithms for the computation of sea surface fluxes using TOGA COARE and TAO DATA. J Climate 11: 2628–2644

Authors' addresses: Daniel Martínez-Castro (e-mail: daniel.martinez@insmet.cu), Arnoldo Bezanilla-Morlot, Lourdes Alvarez-Escudero, Instituto de Meteorología. La Habana, Cuba; Rosmeri Porfirio da Rocha, Universidade de São Paulo, São Paulo, Brasil; Julio Pablo Reyes-Fernández, Centro de Previsão do Tempo e Estudos Climaticos (CPTEC)/Instituto Nacional de Pesquisas Espaciais (INPE), São Paulo Brasil; Yamina Silva-Vidal, Instituto Geofisico del Perú. Lima. Perú; Raymond W. Arritt, Iowa State University, Ames, Iowa, USA.